Powder Technology 205 (2011) 172–183

Contents lists available at ScienceDirect

Powder Technology

journal homepage: www.elsevier.com/locate/powtec

A DEM study on the effective thermal conductivity of granular assemblies

H.W. Zhang [a,*], Q. Zhou [a], H.L. Xing [b], H. Muhlhaus [b]

[a] State Key Laboratory of Structural Analysis for Industrial Equipment, Department of Engineering Mechanics, Faculty of Vehicle Engineering and Mechanics, Dalian University of Technology, Dalian 116024, PR China
[b] Earth System Science Computational Centre, School of Earth Sciences, The University of Queensland, St Lucia, QLD4072, Australia

ARTICLE INFO

Article history:
Received 15 January 2010
Received in revised form 2 September 2010
Accepted 7 September 2010
Available online 17 September 2010

Keywords:
Discrete element method
Effective thermal conductivity
Granular materials
Average heat flux
Average temperature gradient

ABSTRACT

A discrete element method (DEM) is developed to simulate the heat transfer in granular assemblies in vacuum with consideration of the thermal resistance of rough contact surfaces. Average heat flux is formulated by the positions and heat flow rates of particles on the boundaries of the granular assemblies. Average temperature gradient is given as a best-fit formulation, which is computed from the relative position and temperature of particles. With the thermal boundary condition imposed on the border region, the effective thermal conductivity (ETC) of granular assemblies can be calculated from the average heat flux and temperature gradient obtained from DEM simulations. Moreover, the effects of particle size, solid volume fraction and coordination number on the ETC are also investigated. Simulation results show that granular assemblies with coarse particles and under large external compression forces exhibit a better heat conduction behavior. The effects of particle size and external compression forces on the ETC are in good agreement with experiment observations.

1. Introduction

Thermal conductivity of granular assemblies is an important property for many industrial handling processes, including packed bed and multi-phase reactors. At present, some theoretical and semi-empirical methods are used to predict the effective thermal conductivity (ETC) of packed beds [1]. In practice, however, these methods have met difficulties in predicting the ETC influenced by the contact mechanics exhibited by particles in granular assemblies.

Various experimental tests have been performed to measure the thermal conductivity of granular materials and to understand the effect of particle properties. Woodside and Messmer [2] investigated the effect of porosity, solid particle and saturated fluid conductivity on the particulate bed conductivity as early as in 1961. Tavman and Tavman [3] found a linear dependence of the ETC to the moisture content of the particles. Bala et al. [4] investigated the effect of porosity and size on the thermal conductivity. Weidenfeld et al. [5] studied the ETC of particulate beds under compression via experiments and developed a theoretical model based on these data. Their results show a significant effect of the contact area between particles on the effective thermal conductivity. Bahrami et al. [6] developed a heat transfer model for predicting the ETC of a regularly packed bed consisting of uniformly sized spheres based on their previous studies on the thermal conductance between two surfaces [11]. This model is compared with experimental data of heat transfer in sphere assemblies with different diameters and a good agreement is observed.

Compared to experiments, numerical simulations provide an easier solution to predicting the ETC, since the heat exchange and contact information can be easily accounted from the simulation data. Vargas et al. [7] developed a Thermal Particle Dynamic method to investigate the heat transfer within the particle assemblies and performed simulations to study the thermal expansion effects in the granular system [8]. Their results show that a systematic and controllable increase in granular packing can be induced by simply raising and then lowering the temperature without any mechanical energy input, which is in agreement with the experiment [9]. Nguyen et al. [10] modeled the granular flow and heat transfer between particles during the discharge of a silo. The simulation results indicate that both discharge velocity and heat generated by the friction would influence the temperature of particles and affect their flow behavior eventually.

Based on the work mentioned above, we introduce a thermal contact model considered thermal resistance of rough surfaces into a discrete element method (DEM) according to the research of Bahrami et al. [11,12]. Moreover, we derived the average heat flux and the average temperature gradient expressions, respectively. With appropriate thermal and mechanical boundary conditions applied, these two terms can be accounted from simulation data. The ETC of granular assemblies thus can be obtained. The relationship between the ETC and mechanical parameters of granular assemblies is investigated, including stress in the heat transfer direction, average particle diameter, solid volume fraction and coordination number, respectively.

* Corresponding author. Tel./fax: +86 411 84708769.
E-mail address: zhanghw@dlut.edu.cn (H.W. Zhang).

0032-5910/$ – see front matter © 2010 Published by Elsevier B.V.
doi:10.1016/j.powtec.2010.09.008

Nomenclature

A	section area of granular assemblies, m^2
a	contact radius, m
B	Boundary of granular assembly
b	threshold of the time-step selection
C	Set of contacted particles
c	specific heat, J kg^{-1} K^{-1}
d	distance between the two particle centers, m
dt	time-step, s
d_v	Vickers indentation diagonal, μm
E	Young's modulus, Pa
$\mathbf{F}$	force, N
F	magnitude of force, N
H	hardness of the bulk material, Pa
h	thermal conductance, W K^{-1} m^{-2}
$\bar{h}$	thermal conductance with perfectly smooth surfaces, W K^{-1} m^{-2}
I	moment of inertia, kg m^2
K	contact stiffness, N/m
$\mathbf{k}$	thermal conductivity tensor
k	thermal conductivity, W m^{-1} K^{-1}
M	torques, N m
m	mass, kg
N	number of particles
n	normal vector
Q	total heat flow rate, W
q	heat flow rate, W
q''	heat flux, W m^{-2}
$\dot{q}$	heat density, W kg^{-1}
R	thermal resistance, W^{-1} K m^2
$\bar{R}$	ideal thermal resistance, W^{-1} K m^2
R_s	thermal resistance of surface roughness, W^{-1} K m^2
r	particle radius, m
s	mean absolute surface slope
T	temperature, K
t	time, s
$\mathbf{v}$	velocity, m s^{-1}
v	volume of particle, m^3
$\mathbf{u}$	displacement, m

Greek symbols

β	the expansion coefficient
γ	damping ratio
δ	overlap between the two contacted particles, m
η	roughness, m
μ	sliding friction coefficient
ν	Poisson ratio
ρ	density of the particle, kg m^{-3}
$\boldsymbol{\omega}$	angular velocity, rad s^{-1}

Subscripts

B	Brinell
e	effective
min	minimum
n	normal
t	tangential
tot	total

Superscript

i,j	particle i, particle j

2. Modeling

Cundall [13] developed the discrete element method to study the mechanics of granular assemblies. Every degree of freedom of particles is determined by the explicit solution of Newton's equations, which is given by

$$m^i\dot{\mathbf{v}}^i = \sum \mathbf{F}^i \tag{1.a}$$

$$I^i\dot{\boldsymbol{\omega}}^i = \sum \mathbf{M}^i \tag{1.b}$$

in which m^i and $I^i$are the mass and moment of inertia of particle, and $\mathbf{v}^i$ and $\boldsymbol{\omega}^i$ are the particle velocity and particle angular velocity, respectively. $\sum \mathbf{F}^i$ represents the total force applied on particle i, including body force, contact force between contact particles and external force applied on the boundaries of granular assemblies. $\sum \mathbf{M}^i$ represents relevant torques. The contact model is typically determined from contact mechanics considerations [14], most in the Hertzian contact model. Silbert et al. [15] gave the equations that can represent either the linear or Hertzian contact model to compute the normal and tangential contact forces, $\mathbf{F}_n$ and $\mathbf{F}_t$, which are expressed as

$$\mathbf{F}_n = f(\delta/d)(K_n\mathbf{n}_n\delta - \gamma_n m_e\mathbf{v}_n) \tag{2.a}$$

$$\mathbf{F}_t = f(\delta/d)(-K_t\mathbf{u}_t - \gamma_t m_e\mathbf{v}_t) \tag{2.b}$$

where K_n and K_t are the normal and tangential contact stiffness, and γ_n and γ_t are the normal and tangential damping ratio, respectively. δ is the overlap between the two particles. d is the distance between the two particle centers. $\mathbf{n}_n$ is the contact normal vector . $\mathbf{u}_t$ is the relative tangential displacement. $\mathbf{v}_n$ and $\mathbf{v}_t$ are the normal and tangential relative velocity, respectively. $m_e = m^i m^j/(m^i + m^j)$ represents the effective mass of the contact pair.$f(x) = 1$ for the linear spring-dashpot model, or $f(x) = \sqrt{x}$ for Hertzian contacts with viscoelastic damping. The maximum tangential contact force is determined by the Coulomb friction law and its magnitude satisfies

$$|F_t| \le \mu|F_n| \tag{3}$$

where μ is the sliding friction coefficient.

The key feature of the DEM is to model a many-body system by many simultaneous two-body interactions. This is valid only when the time increase is rather small that no disturbance propagates further than a particle's immediate neighbors within one time-step. Hence the time-step is chosen as $br_{\min}/\lambda$ [13], in which $r_{\min}$ is the smallest radius of the particles in granular assemblies, λ is the relevant disturbance wave speed that is determined by Young's modules and density of the particles, and $b \le 1$ is a threshold of the time-step selection.

2.1. DEM for heat conduction analysis

To simulate the thermal conduction in granular assemblies, the temperature must be introduced into the DEM as an additional degree of freedom. Generally, the temperature $T^i(x,y,z,t)$ of each particle (see in Fig. 1) in the system should satisfy the following heat conduction equation

$$\rho^i c^i T^i{}_{,t} - \left(k_1 T^i{}_{,1}\right)_{,1} - \left(k_2 T^i{}_{,2}\right)_{,2} - \left(k_3 T^i{}_{,3}\right)_{,3} - \rho^i \dot{q}^i = 0 \tag{4}$$

and the corresponding boundary conditions are given by

$$\begin{aligned} &\partial P^1 : T = \bar{T} \\ &\partial P^2 : k_1 T^i{}_{,1}\, n_1 + k_2 T^i{}_{,2}\, n_2 + k_3 T^i{}_{,3}\, n_3 = q \\ &\partial P^3 : k_1 T^i{}_{,1}\, n_1 + k_2 T^i{}_{,2}\, n_2 + k_3 T^i{}_{,3}\, n_3 = h(T_a - T) \end{aligned} \tag{5}$$

where ρ^i is the density of the particle materials,c^i is the specific heat, t is time, $\dot{q}^i$ is the heat density, n_1, n_2, and n_3 are the components of

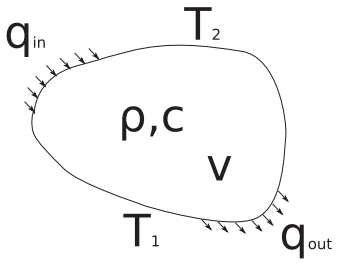

Fig. 1. The schematic of thermal boundary conditions of one particle.

unit vector on the boundaries, $\bar{T} = \bar{T}\left(\partial P^1, t\right)$ is the given temperature on particle boundary ∂P^1, $q = q(\partial P^2, t)$ is the heat flow rate on particle boundary ∂P^2, h is the heat conductance and k is the heat conductivity.

The determination of the temperature field of each particle is very time consuming since granular assemblies in reality contain a huge number of particles. To save the computational cost, thus, each particle has only one temperature degree of freedom in DEM simulations. In addition, it is generally assumed that there is no heat source within the particle, e.g., $\dot{q} = 0$, and all heat transfer with other particles is accounted as boundary conditions. Using $\int_{\partial P}$ to represent the integration on the surface of the particle, the state of one particle can be written as

$$\rho^i c^i v^i T^i{}_{,t} = \int_{\partial P} k_1 T^i{}_{,1}\, n_1 + k_2 T^i{}_{,2}\, n_2 + k_3 T^i{}_{,3}\, n_3 da = q^i \tag{6}$$

in which v^i represents the volume of the particle, q^i represents the total heat exchange between particle i and others. Calculating q^i requires heat exchange q^{ji} between two contact particles, which is given by

$$\begin{aligned} q^{ji} &= \left(T^j - T^i\right) \int_{\partial P} h da \\ &= \left(T^j - T^i\right) h^{ij} \end{aligned} \tag{7}$$

where h^{ij} denotes the heat conductance between the two particles, T^i and T^j the temperatures of particles i and j, respectively. Hence the total heat exchange between particle i and the other N particles can be expressed as

$$\rho^i c^i v^i T^i{}_{,t} = \sum_{j=1}^{N} h^{ij}\left(T^j - T^i\right) \tag{8}$$

Here, the heat conductance h^{ij} is related to heat conductivity, surface contact properties and temperature gradient, and can be computed from one dimensional quasi-steady thermal contact model with two caveats [8]. First, the internal heat transfer is much faster than the external one. Second, the thermal transients are small enough to be quantified as a quasi-steady heat flow. The 1-D problem can thus be expressed as

$$(kT_{,z})_{,z} = 0 \tag{9}$$

in which z denotes the direction of the thermal conduction. The integration of Eq. (9) gives the following Fourier's heat conduction equation,

$$-kT_{,z} = q'' \tag{10}$$

where q'' represents the heat flux. Thus the heat flow rate q^{ji} over an arbitrary section A can be expressed as

$$q^{ji} = \int_A kT_{,z}\, dA = \int_A q'' dA \tag{11}$$

which gives the heat exchange between particles i and j. q^{ji} is determined by the thermal conductance h^{ji}. Eq. (11) can be rewritten as

$$q^{ji} = \int_A q'' dA = h^{ji}\left(T^j - T^i\right) \tag{12}$$

h^{ij}, which is reciprocal to R_{tot}, can be calculated according to the well known definition of heat resistance [1], which is given by

$$h^{ij} = \frac{1}{R_{tot}} = \frac{q^{ij}}{T^j - T^i}. \tag{13}$$

Usually, the thermal conductance can be obtained from FEM simulations or experiments.

On the other hand, Yovanovich [16], Holm [17], and Batchelor and O'Brien [18] have proposed independently the approximate analytical solutions of heat conductance $\bar{h}^{ij}$ with perfectly smooth surfaces, which is presented as

$$\bar{h}^{ij} = \frac{1}{\bar{R}} = 2k\left(\frac{3F_n r_e}{4E_e}\right)^{1/3} \tag{14}$$

where $\bar{R}$ denotes the ideal thermal resistance, F_n is the magnitude of normal contact force between the two contact particles, and k is the thermal conductivity. r_e and E_e are the effective radius and the effective Young's modulus, which are determined by

$$\frac{1}{r_e} = \frac{1}{r^i} + \frac{1}{r^j} \tag{15.a}$$

$$\frac{1}{E_e} = \frac{1-\nu^{i^2}}{E^i} + \frac{1-\nu^{j^2}}{E^j} \tag{15.b}$$

We have performed the two-sphere contact and thermal conduction FEM simulation in commercial software ABAQUS [33], with the particle diameters of $d^i = d^j = 2\times10^{-3}$ m, the thermal conductivity of $k = 1\times10^2$ W m^{-1}K^{-1}, the Young's modulus of $E^i = E^j = 6.98\times10^{10}$ Pa and Poisson ratio $\nu^i = \nu^j = 0.2$. With heat flow data and temperature difference information obtained, the thermal conductance is calculated from Eq. (13). The analytic solution of the same parameters can be obtained from Eq. (14). As shown in Fig. 2, a good match between the analytical and numerical solutions indicates that Eq. (14) can quantify the heat transfer between two contact particles in the DEM accurately, even with a rather large overlap between the two particles. Vargas et al. [7] introduced the heat transfer algorithm into the DEM based on Eq. (14) and named it after the Thermal Particle Dynamic Method. It has been employed to simulate the transient heat conduction in the packed bed of particles. Compared to experiment results [7] and theoretical predictions obtained from a fabric tensor based effective conductivity expression [19], a good qualitative and quantitative agreement for temperature profiles in granular assemblies has been obtained.

2.2. Thermal resistance model between rough surfaces in the DEM

For particles in reality, there are some cracks existing on the surfaces in contact. Xing et al. [23] developed an algorithm for analyzing the transient thermal coupling with the frictional contact between the multiple elastic–plastic bodies using the R-minimum strategy. FEM simulations have demonstrated the efficiency, stability and usefulness of this algorithm. Recently, Bahrami et al. proposed that the rough surface of spherical particles can be regarded as the Gaussian rough surface, and the contact between these two surfaces can be modeled by a smooth Gaussian surface and a rough surface with two different rough characteristics combined together [11,12]. The thermal resistance of rough surface R_s can be described as a

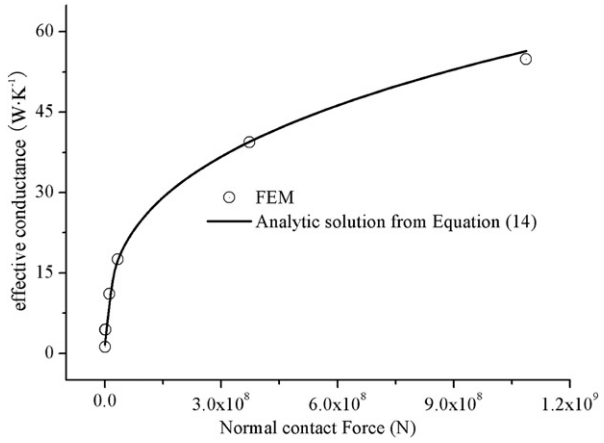

Fig. 2. The comparison between Eq. (14) and $\bar{h}^{ij}$ calculated by Eq. (13) based on the FEA result. Eq. (14) is shown in solid line.

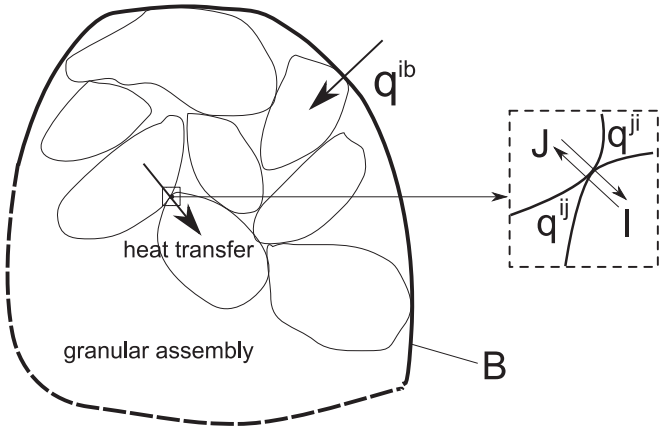

Fig. 3. The schematic of heat transfer in granular assemblies.

function of the combined roughness $\eta = \sqrt{\eta^{i2} + \eta^{j2}}$ and the surface slope $s = \sqrt{s^{i2} + s^{j2}}$, which is given by

$$R_s = \frac{0.565H^*(\eta/s)}{kF_n} \tag{16}$$

where $H^* = c_1(\eta'/s)^{c_2}$, $\eta' = \eta/\eta_0$ and $\eta_0 = 1$ μm. The relationship between η and s is [21]

$$s = 0.152\eta^{0.4}. \tag{17}$$

while c_1 and c_2 are determined by the microhardness and can be fitted by two empirical expressions as

$$\begin{aligned} c_1 &= H_{BGM}\left(4.0 - 5.77\kappa + 4.0\kappa^2 - 0.61\kappa^3\right) \\ c_2 &= -0.57 + 0.82\kappa - 0.41\kappa^2 + 0.06\kappa^3 \end{aligned} \tag{18}$$

in which $\kappa = H_B/H_{BGM}$, H_B is the Brinell hardness of the bulk material with a value of $H_{BGM} = 3.178$ GPa [6,20]. The correlations in Eq. (18) are valid for the range of $H_B \in [1.3, 7.6]$GPa. When an effective value of microhardness $H_{mic} = c_1(d_v/\eta_0)^{c_2}$ is known, in which d_v is the Vickers indentation diagonal, the Vickers microhardness parameters will be $c_1 = H_{mic}$ and $c_2 = 0$. A detailed expression of this model for heat resistance with surface roughness and its applications can be found in the works of Bahrami et al. [6,11,12,20].

According to the definition of the heat resistance, the rough and ideal thermal resistance can be accounted together to quantify the heat conduction between the two particles, which is given by

$$R_{tot} = R_s + \bar{R}. \tag{19}$$

Eq. (19) implies that $h^{ij}$is smaller than $\bar{h}^{ij}$.

According to the above discussions, a many-body heat transfer system can be modeled by many simultaneous two-body interactions with computing the heat exchange from Eq. (19) and updating every particle's temperature according to Eq. (8), as depicted in Fig. 3. A requirement is that the temperature of each particle changes so little that thermal disturbances do not propagate further than its immediate neighbors in one time-step. This criterion can be shown to be met by choosing a time-step dt which satisfies [7]:

$$\frac{dt}{\rho c v R_{tot}} << 1. \tag{20}$$

In this work, the magnitude of dt is chosen as $dt \approx 10^{-3} - 10^{-2}$s, depending on the material parameters and size of the particles. It should be noted that the chosen dt in the thermal DEM simulation is often orders of magnitude larger than the analogous time-step in the DEM. The time-step in simulations combined kinematics and thermal conduction is often chosen as indicated in DEM analyses [13].

3. Effective thermal conductivity

To obtain the ETC of granular assemblies, a simple way is to get heat flux and temperature gradient in DEM simulations then solve the equation of Fourier's law of heat conduction. Therefore, we need the technique to obtain these two terms. At the granular assembly level, the methodology to obtain average stress and strain in granular assemblies has been talked about in many studies. The expressions of average stress/couple-stress tensor have been derived based on the balance of internal and external forces applied on the granular assemblies as well as the virtual work principle [24–26]. On the other hand, the strain tensor can be obtained by defining a translation gradient tensor that gives the smallest deviation from the characteristic displacement of the assemblies [13,27–29]. Analogously, the average heat flux and temperature gradient can be obtained from the information of granular assemblies.

Fig. 3 shows a granular assembly in vacuum with contiguous collection of particles that could be a cluster of particles or just a subregion of granular materials. Since we are discussing heat conduction of granular materials in steady state, the particles in it satisfy the conditions as follows:

State of equilibrium

The position would not change during the heat conduction procedure, hence there is no heat generated by the friction between particles.

State of heat equilibrium

With the assumption of no heat source within the granular assembly, the temperature of each particle does not change when it reaches the state of heat equilibrium. In this study, the thermal DEM simulation is performed until the heat flows into, q_{in}, and out of the granular assemblies, q_{out}, are the same, which is expressed as

$$\frac{q_{out} - q_{in}}{q_{in}} < \zeta \tag{21}$$

where ζ is a small number, for this work chosen as $\zeta = 10^{-4}$.

Granular materials in vacuum

There is no medium in the void of the granular materials. Assuming no radiation between particles, the only form of thermal conduction thus is the heat exchange through the contact pairs.

In the granular assembly, the relative coordinate $\mathbf{x^i}$ of the particles is defined as

$$\mathbf{x^i} = \mathbf{X^i} - \mathbf{X^0} \tag{22}$$

in which $\mathbf{X^i}$ is the global coordinate of the particles. The referenced point $\mathbf{X^0}$ is an arbitrary one and it is generally chosen as the average position vector of the N particles of the granular assembly, of which the coordination is given by

$$\mathbf{X^0} = \frac{1}{N}\sum_{i\in R}\mathbf{X^i} \tag{23}$$

in which R denotes the granular assembly. Analogously, the reference temperature T^0 is defined as the average over the temperature T^i of the N particles, which is formulated as

$$T^0 = \frac{1}{N}\sum_{i\in R} T^i. \tag{24}$$

Here, T^0 is used to define the relative temperature $\hat{T}^i$ of each particle in granular materials, which is expressed as

$$\hat{T}^i = T^i - T^0. \tag{25}$$

The parameters mentioned above, together with the heat exchange information among the particles, are the available features to compute average heat flux and average temperature gradient, both of which are required variables to calculate the ETC. In the following sections, detailed derivations are given to formulate the calculation of average heat flux and average temperature gradient.

3.1. Average heat flux

In this study, only the thermal conduction is accounted so that the change of internal energy ΔU^i of particle i is expressed as

$$\Delta U^i = \int_t \int_P \rho^i c^i T^i{}_{,t}\, dP dt \tag{26}$$

where $\int_P$ and $\int_t$ represent the integration on the particle and in the time domains, respectively. According to the equilibrium states mentioned above, there is no work done by the particles so that ΔU^i is only related to the total heat flow q^i on the surface of particle i. The rate of internal energy $\Delta U^i{}_{,t}$ of the particle thus reads

$$\Delta U^i{}_{,t} = q^i = \int_{\partial P} \mathbf{q}''^{(i)} \cdot \mathbf{n}^i da \tag{27}$$

in which $\mathbf{q}''^{(i)}$ is the heat flux on the surface of the particle and $\mathbf{n}^i$ is the outward oriented unit surface normal. In granular materials, q^i is accounted from the total heat exchange q^{ic} between particle i and other particles, as well as the total heat q^{ib} flowing through the boundary contacting with particle i, if any. Hence Eq. (27) can be expressed as an equivalent form as

$$q^i = q^{ic} + q^{ib} \quad \begin{cases} q^{ib} = 0 & i \notin B \\ q^{ib} \neq 0 & i \in B \end{cases} \tag{28}$$

in which B denotes the boundary of the granular assembly. q^{ic} and q^{ib} are computed from

$$q^{ic} = \sum_{j\in C^i} q^{ij} \tag{29.a}$$

$$q^{ib} = \sum_{j\in B^i} q^{ij} \tag{29.b}$$

in which C^i and B^i represent the contacts and local boundaries of the particle i, respectively. Noticing that T^i does not change when the granular system is in the state of heat equilibrium, i.e., $T^i{}_{,t} = 0$, the combination of Eqs. (26), (27) and (28) yields

$$q^{ic} + q^{ib} = 0. \tag{30}$$

Eq. (30) describes the state of an individual particle within the granular assembly in the state of heat equilibrium. The temperature of every particle thus remains constant so that the sum of heat exchange of the granular assembly reads

$$\sum_{i\in R} \int_P \rho^i c^i T^i{}_{,t}\, dP = \sum_{i\in R} q^i = 0. \tag{31}$$

Under this condition, the total heat exchange through the boundary of the granular assembly is 0. Hence Eq. (31) can be expressed equivalently using the heat flux $\mathbf{q}''$ flowing through the boundaries, which is given by

$$\int_{\partial R} \mathbf{q}'' \cdot \mathbf{n} da = 0 \tag{32}$$

where $\mathbf{n}$ and $\int_{\partial R}$ represent the outward oriented unit boundary normal and the integration on the boundary of the granular assembly, respectively. An equivalent form of Eq. (32) can be expressed as the total heat exchange between the particles and the boundary, which is a discrete form expressed as

$$\int_{\partial R} \mathbf{q}'' \cdot \mathbf{n} dA = \sum_{i\in B} q^{ib} = 0. \tag{33}$$

The average heat flux $\langle \mathbf{q}'' \rangle$ of the granular assembly is accounted from the heat flux within it, which is given by

$$\left\langle \mathbf{q}'' \right\rangle = \frac{1}{V_R}\int_R \mathbf{q}'' dV \tag{34}$$

where V_R is the volume of the granular assembly and $\int_R$ represents the integration within it. As a vector, $\mathbf{q}''$ satisfies

$$(\mathbf{q}'')^T = \mathbf{I}(\mathbf{q}'')^T = \left(\nabla \mathbf{x}^i\right)(\mathbf{q}'')^T \tag{35.a}$$

$$\nabla\cdot\left(\mathbf{x}^i \otimes \mathbf{q}''\right) = \left(\nabla \mathbf{x}^i\right)(\mathbf{q}'')^T + \mathbf{x}^i \otimes (\nabla\cdot\mathbf{q}'') \tag{35.b}$$

in which ∇ and $\otimes$ represent vector operator and dyad of two vectors, respectively. The insertion of Eq. (35.a) to (35.b) yields

$$(\mathbf{q}'')^T = \nabla\cdot\left(\mathbf{x}^i \otimes \mathbf{q}''\right) - \mathbf{x}^i \otimes (\nabla\cdot\mathbf{q}''). \tag{36}$$

Eq. (34) can thus be rewritten as

$$\langle \mathbf{q}'' \rangle^T = \frac{1}{V_R}\int_R \nabla\cdot\left(\mathbf{x}^i \otimes \mathbf{q}''\right) dV - \frac{1}{V_R}\int_R \mathbf{x}^i \otimes (\nabla\cdot\mathbf{q}'') dV. \tag{37}$$

The consideration of heat equilibrium in granular materials gives [1]

$$\nabla\cdot\mathbf{q}'' = 0. \tag{38}$$

Submitting Eq. (38) to Eq. (37), the second term of Eq. (37) vanishes so that the average heat flux is expressed as

$$\left\langle \mathbf{q}'' \right\rangle^T = \frac{1}{V_R}\int_R \nabla\cdot\left(\mathbf{x}^i \otimes \mathbf{q}''\right) dV. \tag{39}$$

with the Gauss integration theorem, average heat flux is formulated as

$$\langle \mathbf{q}'' \rangle^T = \frac{1}{V_R} \int_{\partial R} \mathbf{x}^i \otimes \mathbf{q}'' \cdot \mathbf{n} dA \tag{40}$$

that is

$$\langle \mathbf{q}'' \rangle = \frac{1}{V_R} \int_{\partial R} \mathbf{q}'' \cdot \mathbf{n} \otimes \mathbf{x}^i dA. \tag{41}$$

with the heat exchange integration on the boundary taken place by the sum of heat exchange of all the individual particles contacting with the boundary, Eq. (41) can be reformulated as

$$\langle \mathbf{q}'' \rangle = \frac{1}{V_R} \sum_{i \in B} q^{ib} \mathbf{x}^i. \tag{42}$$

Eq. (42) gives the equation that computes the average heat flux of the granular assembly.

3.2. Average temperature gradient

The approximate temperature $\tilde{T}^i$ of each particle can be expressed as a function of temperature gradient ∇T and the particle position, which is given by

$$\tilde{T}^i = \nabla T \cdot \mathbf{x}^i. \tag{43}$$

In consideration of the fluctuation of the temperature distribution within the granular assembly, the relative temperature $\hat{T}^i$ cannot be computed from Eq. (43) exactly, which is expressed as

$$\hat{T}^i - \nabla T \cdot \mathbf{x}^i \neq 0. \tag{44}$$

Now let us find the specific $\langle \nabla T \rangle$ for that the square sum of the deviations in Eq. (44) is the smallest, which can be expressed as,

$$Y = \sum_{i \in R} \left(\hat{T}^i - \langle \nabla T \rangle \cdot \mathbf{x}^i \right)^2 \to \min. \tag{45}$$

The function Y is minimal when it satisfies,

$$\frac{\partial Y}{\partial \langle \nabla T \rangle} = 0. \tag{46}$$

Hence $\langle \nabla T \rangle$ can be obtained as a solution of the linear equations that is given by

$$\sum_{i \in R} \mathbf{x}^i \left(\hat{T}^i - \langle \nabla T \rangle \cdot \mathbf{x}^i \right) = 0 \tag{47}$$

which is the "best-fit" form of the average temperature gradient.

3.3. Effective thermal conductivity

The constitutive relation between the heat flux $\mathbf{q}''$ and the temperature gradient ∇T is given by Fourier's law of heat conduction

$$\mathbf{q}'' = -\mathbf{k} \cdot \nabla T \tag{48}$$

in which $\mathbf{k}$represents the thermal conductivity of materials. In physical tests, $\mathbf{k}$ can be calculated from the given temperature difference and measured heat flow in the direction of conduction, as solving an inverse problem. For thermal conduction in the granular materials, we simply replace $\mathbf{k}$ with the effective thermal conductivity $\mathbf{k_e}$, then Eq. (48) is rewritten as

$$\langle \mathbf{q}'' \rangle = -\mathbf{k_e} \cdot \langle \nabla T \rangle \tag{49}$$

in which the average heat flux $\langle \mathbf{q}'' \rangle$ and the average temperature gradient $\langle \nabla T \rangle$ within the granular assembly can be obtained from Eqs. (42) and (47).

As many researchers pointed out, the boundary conditions applied on the local problem for computing the upscale permeability tensors may have an impact on the accuracy of the calculation results. As illustrated in Fig. 4, the target block plus border regions are used to compute $\mathbf{k_e}$ of granular assemblies, which is used in an upscaling technique to get a more accurate equivalent permeability tensor in heterogeneous materials [27,28]. Here we use the Dirichlet boundary condition for the solution of the extended local problems [27,29], in which the temperature boundary condition is imposed on the target block plus border regions thus heat flux information can be obtained.

Tensor $\mathbf{k_e}$ is further required to be symmetry and positive definite. The recent research [27,30–32] indicates that both of these constrains are automatically satisfied in the great majority of cases by enforcing the symmetry of $\mathbf{k_e}$. Then $\mathbf{k_e}$ can be obtained from solving the following overdetermined linear system that is given by

$$\begin{bmatrix}
{}^1T_{,1} & {}^1T_{,2} & {}^1T_{,3} & & & & & & \\
 & & & {}^1T_{,1} & {}^1T_{,2} & {}^1T_{,3} & & & \\
 & & & & & & {}^1T_{,1} & {}^1T_{,2} & {}^1T_{,3} \\
{}^2T_{,1} & {}^2T_{,2} & {}^2T_{,3} & & & & & & \\
 & & & {}^2T_{,1} & {}^2T_{,2} & {}^2T_{,3} & & & \\
 & & & & & & {}^2T_{,1} & {}^2T_{,2} & {}^2T_{,3} \\
{}^3T_{,1} & {}^3T_{,2} & {}^3T_{,3} & & & & & & \\
 & & & {}^3T_{,1} & {}^3T_{,2} & {}^3T_{,3} & & & \\
 & & & & & & {}^3T_{,1} & {}^3T_{,2} & {}^3T_{,3} \\
 & 1 & & -1 & & & & & \\
 & & 1 & & & & -1 & & \\
 & & & & & 1 & & -1 &
\end{bmatrix}
\begin{Bmatrix} k_{11}^{eq} \\ k_{12}^{eq} \\ k_{13}^{eq} \\ k_{21}^{eq} \\ k_{22}^{eq} \\ k_{23}^{eq} \\ k_{31}^{eq} \\ k_{32}^{eq} \\ k_{33}^{eq} \end{Bmatrix}
= -
\begin{Bmatrix}
{}^1\langle q'' \rangle_1 \\ {}^1\langle q'' \rangle_2 \\ {}^1\langle q'' \rangle_3 \\ {}^2\langle q'' \rangle_1 \\ {}^2\langle q'' \rangle_2 \\ {}^2\langle q'' \rangle_3 \\ {}^3\langle q'' \rangle_1 \\ {}^3\langle q'' \rangle_2 \\ {}^3\langle q'' \rangle_3 \\ 0 \\ 0 \\ 0
\end{Bmatrix} \tag{50}$$

where all blank factors are 0 and the superscripts 1, 2 and 3 represent the boundary problem in the three directions of the Cartesian coordinate system, respectively. All the information required calculating $\langle \mathbf{q}'' \rangle$ and $\langle \nabla T \rangle$ from Eqs. (42) and (47) can be obtained from simulation results and the system is solved as a linear least-squares problem.

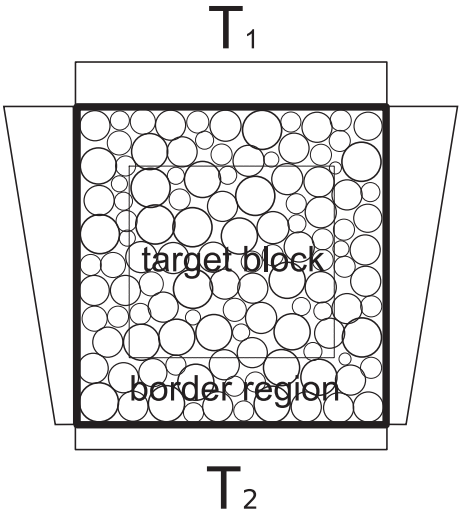

Fig. 4. The schematic of temperature boundary conditions imposed on the granular assembly.

4. Simulations and discussion

The following simulations are performed using our own DEM code, on a PC with Intel® CPU Core™2 duo E6550. Since there are not many particles in the assemblies, the thermal conduction simulation takes few hours to finish the simulation for each case.

4.1. The Effect of the thermal resistance of surface roughness

In this section, the effect on the heat conduction of thermal resistance considered surface roughness is studied both in regularly and randomly packed granular assemblies consisting of spherical particles.

4.1.1. Heat conduction simulation in regularly packed particle specimen

A granular assembly consisting of 11 particles in a row is simulated, as shown in Fig. 5. The model parameters are given in Table 1. All particles are perfectly smooth except the contact surface between particles 6 and 7, of which Vickers microhardness $c_1 = 2.3\times10^9$ Pa and surface roughness $\eta = 0.13$ μm. A compression strain of $\varepsilon_{xx} = -1.0\times10^{-3}$ is applied, then a 10 K temperature difference is imposed on the boundaries with $T_{x=-1\text{mm}} = 283$ K and $T_{x=21\text{mm}} = 273$ K, until the granular assembly reaches its steady state. We perform the DEM simulations using our code and the FEM simulation with ABAQUS [33]. The DEM and FEM temperature profiles are compared in Fig. 5, in which only the temperatures on the centers of spheres are plotted. The temperature discontinuity between particles 6 and 7 illustrates that the rough contact resistance affects the profile of the temperature within the granular assembly. The good agreement between DEM and FEM results indicates that DEM can accurately simulate the heat transfer problem with the consideration of thermal resistance of rough surfaces. Furthermore, DEM is a more efficient method than FEM, e.g., it took only seconds in DEM but hours in FEM to solve this heat-contact problem.

4.1.2. Simulating analysis on randomly packed granular assemblies

A granular assembly consisting of 1106 spheres is restrained in a rectangle region by rigid walls, as shown in Fig. 6. The sizes of the particles follow a normal distribution with an average diameter of $d = 4\times10^{-3}$ m and a standard deviation of 0.25d. The material properties are listed in Table 1. Each rigid wall has its own mass so that it can be driven by the resultant force of external compressions and collisions with inside particles. However, their rotation is prohibited in order to keep the granular assembly to be rectangle

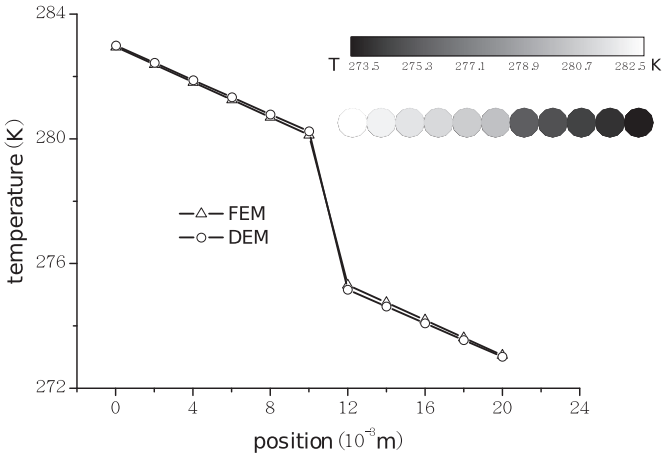

Fig. 5. The comparison between FEM and DEM results of the temperature profile in 11 particle specimen.

Table 1
Material parameters.

Parameter	Value
Density	2.7×10^3 kg m^{-3}
Young's modulus	6.89×10^{10} Pa
Poisson ratio	0.23
Conductivity	1.0×10^2 Wm^{-1}K^{-1}
Specific heat	8×10^2 J kg^{-1} K^{-1}
Friction coefficient	0.5
Expansion coefficient	0.0
Vickers microhardness	2.3×10^8 Pa
Surface roughness (for rough surface only)	0.13×10^{-6} m

during the simulation. Furthermore, the walls have their own degrees of temperature freedom and the heat can flow through them, the temperature difference can be thus applied on the assembly and the heat flow rate can be accounted in every time-step during the simulation. In the current case, a constant temperature difference 1 K (273–274 K) is applied on the boundaries in the x direction. The final temperature profile is shown in Fig. 6b.

The contact force network (force chains) is plotted in Figs. 6c and 6e, in which the thickness of each line section represents the magnitude of the contact forces. The contact force network does not change during the heat transfer procedure of the simulation because all the particles in the specimen have stopped moving before any thermal boundary conditions are applied and that the heat transfer does not bring any mechanical disturbance into this granular system with the expansion coefficient $\beta = 0$. The heat transfer network is plotted in Figs. 6d and f with the line section thickness representing the magnitude of heat flow rate between each contact pair. By comparing these plots, it can be seen that the morphology of the heat conduction network is the same as that of the contact force network. However, the line thickness is different since the heat flow rate between particles depends not only on the magnitude of contact normal forces, but also on other parameters, such as temperature difference of every contact pair. For we are discussing the granular assemblies in vacuum with the heat radiation of particles ignored, the heat conduction path coincides with the contact force network. This observation indicates that the heat conduction is closely related to the contact network and could provide some necessaries to understand the thermal conduction mechanism in the granular assemblies, as contact force network does for the mechanical ones.

The contact interface properties can play important roles in the heat transfer process of a granular assembly as illustrated in the previous regularly packed problem. To investigate the effect of the thermal rough resistance on the effective heat conductivity k_e in an arbitrary direction, say the x direction in this work, detailed DEM simulations are performed, in which all material properties are unchanged except that the Vickers microhardness coefficients are set as $c_1 = 2.3\times10^9$ Pa, $c_1 = 2.3\times10^8$ Pa and $c_1 = 2.3\times10^7$ Pa, respectively. As shown in Fig. 7, k_e decreases with the increase of the Vickers microhardness coefficient under the same compression force, that is, k_e decreases with the increase of R_s. For R_s and $\bar{R}$ are connected in series, the ETC will be almost zero when R_s approaches infinite large, which indicates that the contact surface is extremely rough, while the ETC will be dominated by the value of $\bar{R}$ when R_s is nearly zero, which responds a nearly ideal contact condition. This illuminates that a good heat conduction property of a granular assembly depends on both good material heat conductivity and fine contact condition between particles.

4.2. The influence on effective heat conductivity of the features in granular materials

Besides material properties, the ETC can be determined by the external loads and the geometric parameters, such as particle size,

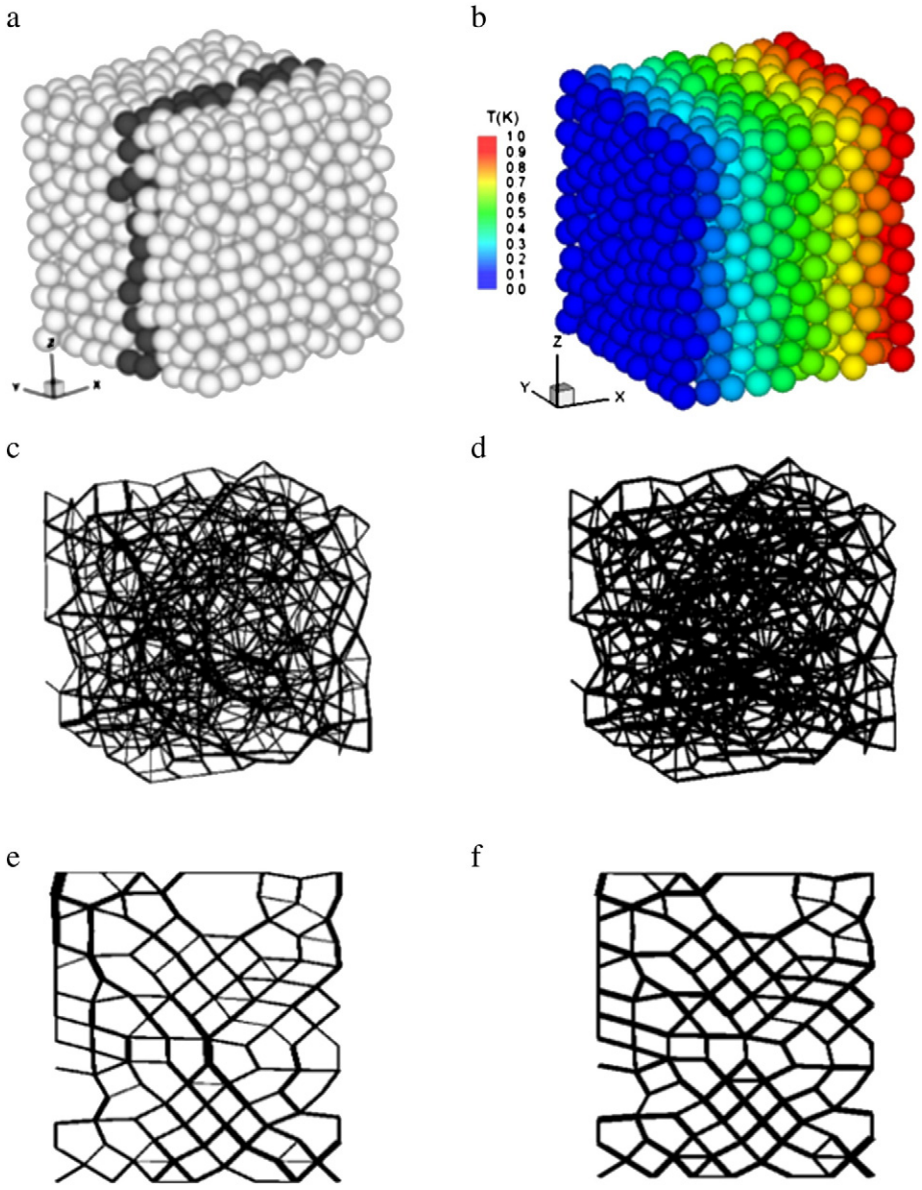

Fig. 6. The schematic of a granular assembly consisting of 1106 particles; a) Particle arrangement within the assembly, the force and heat transfer network schematics in e) and f) are plotted in the dark particle layer; b) The temperature profile within the assembly (only the relative temperature to the reference temperature 273K is depicted) ; c) The force chains; d) The heat transfer network; e) The force chains in the dark particle layer shown in a); f) The heat transfer in the dark particle layer shown in a).

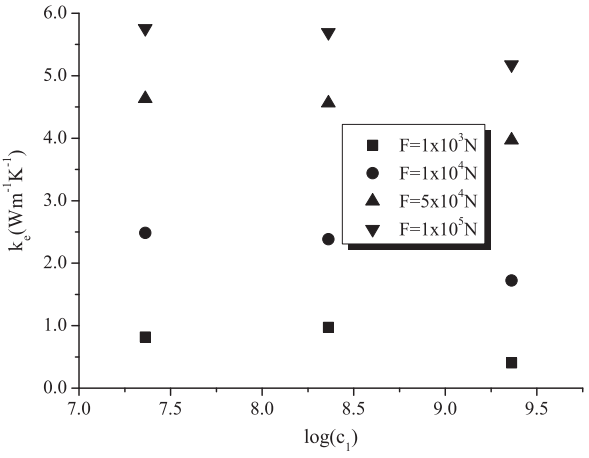

Fig. 7. The effect of rough surface properties on k_e.

solid volume fraction and coordination number. In Sections 4.2.1, 4.2.2 and 4.2.3, we will discuss the effects on the ETC of these parameters respectively, assuming that other parameters remain constant in every theoretical and numerical analysis. In section 4.2.4, the combined effect of the parameters investigated is analyzed by detailed DEM simulations.

4.2.1. External loads

Fig. 8 is the schematic of the granular assembly consisting of 18,112 spheres with an average diameter of $d = 6 \times 10^{-3}$ m and a standard deviation of 0.25d. Different compressive loads are applied on this assembly in a set of DEM simulations. As shown in Fig. 9, k_e increases with the increase of the average stress σ_{xx} in the heat conduction direction. Here the average stress is calculated from the positions of particles and the contact forces between particles, which are the reflections of the external compression loads [24–26]. According to Eqs. (14) and (16), micro contact characteristics $\bar{h}^{ij}$ and R_s are dominated by the contact forces. Moreover, k_e is determined by

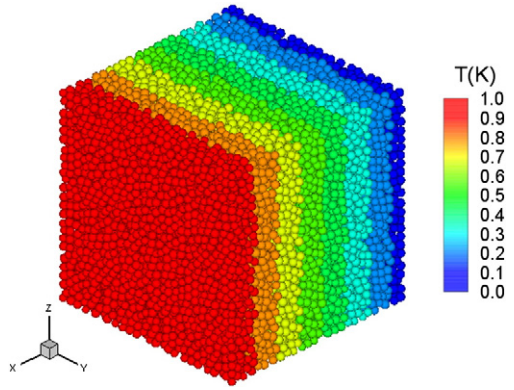

Fig. 8. The temperature profile within the granular assembly. The temperature given is the difference from the reference temperature 273 K.

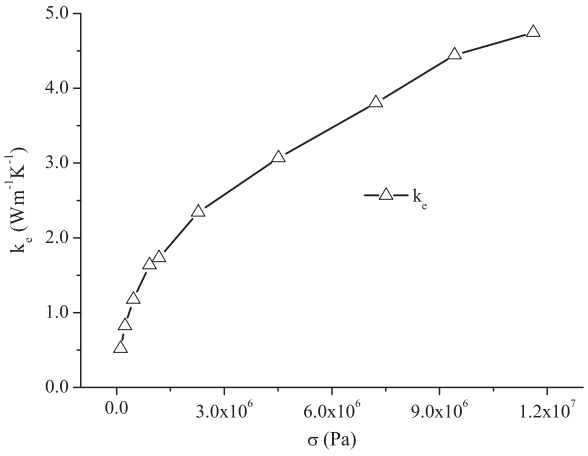

Fig. 9. The evolution of effective thermal conductivity k_e under different compressive loads. Each data point represents the $k_e$responding to a compression stress level.

$\bar{h}^{ij}$ and R_s of every individual contact pair. Thus k_e is logically related to the external compression loads. From the above analysis, it can be concluded that a greater external load would lead to a larger k_e when material properties and geometric parameters are unchanged in granular assemblies.

4.2.2. Particle size

The simple cubic arranged granular assemblies (see in Fig. 10) are used to investigate the particle size effect on the overall thermal conduction properties of granular assemblies. By replacing the coarse particles with fine ones of the same total mass, both the particle radii and the contact forces decrease while solid volume fraction and the

Table 2
The comparison of the ETC of simple cubic arranged granular assemblies, with smooth or rough surface.

Number of particle in granular assemblies	k_e(W m^{-1} K^{-1})	
	Smooth	Rough
8 (diameter is 8×10^{-3} m)	2.8184	1.9992
64 (diameter is 4×10^{-3} m)	2.8184	1.5490
512 (diameter is 2×10^{-3} m)	2.8184	1.0679

materials properties remain constant in these assemblies. k_e can be represented by the thermal conduction property of the two-particle contact pair, which is expressed as

$$k_e = \frac{1}{R_{tot}D} \tag{51}$$

in which D represents the diameter of the particle. Substituting Eqs. (14), (16) and (19) to (51), it can be rewritten as

$$k_e = \left(\underbrace{D\left(2k\left(\frac{3F_n r_e}{4E_e}\right)^{1/3}\right)^{-1} + D\frac{0.565H^*(\eta/m)}{kF_n}}_{\tilde{H}} \right)^{-1}. \tag{52}$$

Using n^3 particles with a radius of D/n, two changes will occur in Eq. (52) as follows:

1. the effective radius changes to r_e/n
2. the normal contact force now is F_n/n^2

Substituting these two terms into $\tilde{H}$ in Eq. (52), $\tilde{H}$ can be rewritten as

$$\begin{aligned}\tilde{H} &= D\left(2k\left(\frac{3F_n r_e}{4E_e}\right)^{1/3}\right)^{-1} + D\frac{0.565H^*(\eta/m)}{kF_n} \\ &= \frac{D}{n}\left(2k\left(\frac{3\left(F_n/n^2\right)(r_e/n)}{4E_e}\right)^{1/3}\right)^{-1} + \frac{D}{n}\frac{0.565H^*(\eta/m)}{kF_n/n^2} \\ &= \underbrace{D\left(2k\left(\frac{3F_n r_e}{4E_e}\right)^{1/3}\right)^{-1}}_{G_0} + n\cdot\underbrace{D\frac{0.565H^*(\eta/m)}{kF_n}}_{G_1}.\end{aligned} \tag{53}$$

Noticing that the material parameters remain constant, Eq. (53) can be rewritten as

$$\tilde{H} = G_0 + nG_1. \tag{54}$$

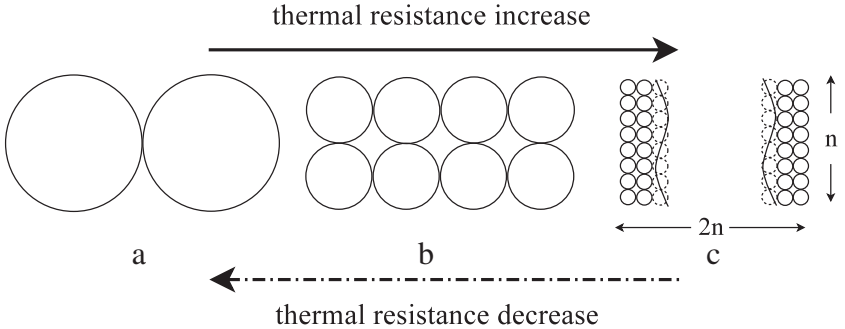

Fig. 10. Scaling dependence of regular packed granular assembly. The temperature difference is applied on the rigid walls in a horizontal direction. The identical compression forces acting on the walls of each specimen.

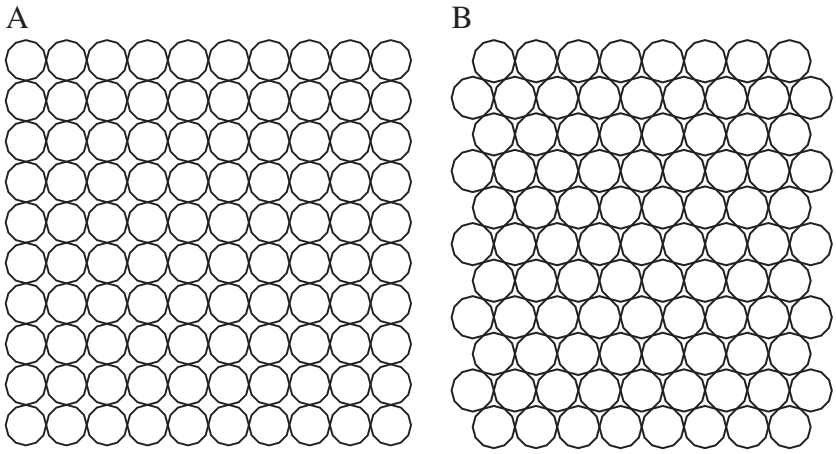

Fig. 11. Two dense granular assemblies, in which the particles are arranged regularly, are applied with identical temperature difference and compression load to investigate the effect of solid volume fraction and coordination number.

Substituting Eq. (53) to (51), it can be reformulated as

$$k_e = \frac{1}{G_0 + nG_1}. \tag{55}$$

Eq. (55) indicates that the ETC of granular assemblies decreases with the increase of factor n, i.e., with the decrease of particle size. This is a direct result of the increase of the number of the thermal resistance and the decrease of contact force in granular assemblies. It should be noted that the ETC of the two-particle contact pair would be a constant value if the contact surfaces are perfectly smooth ($G_1 = 0$ in Eq. (55)), whatever the particle size increase or not. The DEM simulation data is given in Table 2, comparing the ETC of several cases of smooth and rough contact surfaces.

4.2.3. Solid volume fraction and coordination number

It should be noted that only a constant solid volume fraction of the granular assemblies is considered in the above discussion. One question may be raised immediately of how the solid volume fraction affects the effective thermal resistance of granular assemblies. From an empirical impression, dense granular assemblies may have better heat conduction properties than loose ones. This can be verified by simulating two different regular arranged granular assemblies consisting of same size particles, in which identical forces are applied on the boundary walls, as shown in Fig. 11. All material parameters in the two simulations are the same except that B has a larger solid volume fraction than A. The data of k_e and solid volume fraction are compared in Table 3. The simulation results show that the k_e of assembly B is larger than A, which confirms that denser granular assemblies with same size particles under the same compression have better heat conduction properties.

Coordination number is another characterization of the heat conduction property of granular assemblies, which represents the average number of the nearest neighbors of the particles. Greater coordination number results in a larger number of heat transfer "channels" that provide more chance for heat to flow through granular assemblies. Generally, a dense granular assembly has a larger coordination number than a loose one, for example, assembly B's coordination number is greater than A. According to the comparison between B and A, granular assemblies with greater coordination number will exhibit better heat conduction behaviors when the particle size and external compression load are the same.

Table 3a
The comparison of k_e and solid volume fraction between granular assembly A and B.

	Solid fraction	k_e(W m^{-1} K^{-1})
A	52.36%	0.167
B	72.61%	0.237

[a]The schematic of A and B is shown in Fig. 11.

4.2.4. The combined effect of particle size, solid volume fraction and coordination number

Different size particles are arranged randomly in seven groups of granular assemblies, in which the particle diameters are in the range of 4×10^{-3} m$<d<9\times10^{-3}$ m, as presented in Fig. 12. The material properties and total mass of the particles in every granular assembly are shown in Table 1. Due to the stochastic nature of the system, each case is simulated 10 times with a different initial packing. The random distribution of particles leads to different solid volume fractions in these assemblies compressed with the same force. The simulation results of k_e, solid volume fraction and coordination number vs. particle size are illustrated in Figs. 13 and 14, respectively, in which the parameters are averaged over the results of 10 different initial packing.

As shown in these two figures, the tendency of k_e increases but the trend of solid volume fraction and coordination number decreases with the increase of particle size. Noticing the observations in sections 4.2.2 and 4.2.3, the overall increasing tendency of k_e indicates that particle size is dominative to the evolution of k_e. However, the k_e of several individual cases oscillates, such as $k_e = 6.283$ W m^{-1} K^{-1} of case $d = 5.5\times10^{-3}$ m and $k_e = 6.267$ W m^{-1} K^{-1} of case $d = 6\times10^{-3}$ m(not shown in Figs. 13 and 14), which indicates that the decrease of solid volume fraction and coordination number also contributes to the evolution of k_e. The above discussion indicates that the evolution of k_e is a result of competition of the three parameters, including particle size, solid volume fraction and coordination number.

5. Conclusion

In this paper, a series of numerical simulations have been performed to investigate the thermal conduction in granular materials. The thermal resistance of the rough surface model is introduced into a DEM to get more realistic simulation results. The comparison between the DEM and FEM simulations indicates that the DEM can simulate the heat transfer effectively. We have derived the expressions of average heat flux and average temperature gradient of granular assemblies. With these two terms obtained from simulation data, the ETC can be obtained, which presents the heat transfer properties of granular assemblies in steady state. Then the effects of various granular assembly parameters on the ETC are investigated via

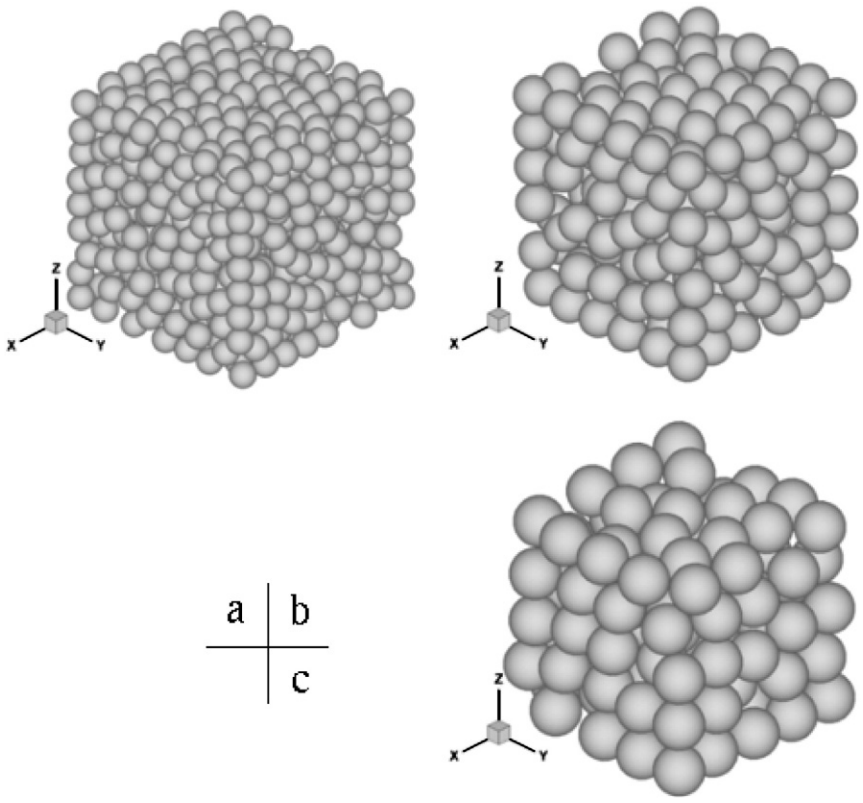

Fig. 12. The schematic of granular assemblies with the same total mass but different size particles. a) $d=4.5\times10^{-3}$ m; b) $d=6.0\times10^{-3}$ m; and c) $d=7.5\times10^{-3}$ m.

detailed DEM simulations, including the external compression force, particle average diameter, solid volume fraction and coordination number. Several observations have been obtained and can be summarized as follows.

1) k_e of the granular assemblies with unchanged morphology increases with the increase of the external compression loads. This coincides with the empirical impression and is in agreement with the experiment of Weidenfeld et al. [22]. While k_e would be infinitely close to a limited value, which would be the thermal conductivity of particle materials, under a very big external compression. This situation goes beyond the appliance of DEM simulations.

2) k_e increases with the enlargement of the particle size in the assemblies with the same external compression load, solid volume fraction and coordination number, which also coincides with the experimental observations [22]. It directly reflects additional thermal resistance for small particles. Moreover, the decrease of contact force enhances the thermal resistance of contact pairs in granular assemblies.

3) k_e increases with the increase of solid volume fraction and coordination number in the assemblies consisting of same size particles size with the same external compression load. This observation may be helpful to improve the thermal conduction properties under the condition that external load and particle size cannot be increased easily.

The combined effect of these parameters investigated, however, indicates that any one be the decisive factor to the evolution of k_e. From a practice view, a *dense* granular assembly consisting of relative *large* particles will exhibit good heat transfer behaviors under *heavy* compressions.

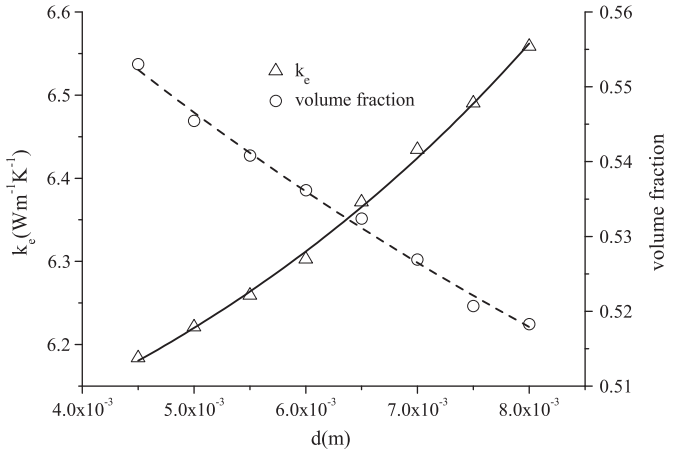

Fig. 13. k_e and solid volume fraction vs. particle size in the assemblies consisting of uniform particles. The solid curve is the trend line of k_e. The dash curve is the trend line of solid volume fraction.

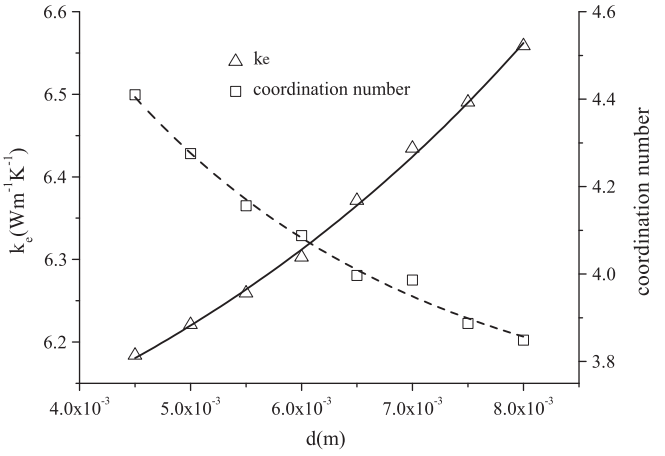

Fig. 14. k_e and solid volume fraction vs. particle size in the assemblies consisting of uniform particles. The solid curve is the trend line of k_e. The dash curve is the trend line of coordination number.

Acknowledgements

The supports of the National Natural Science Foundation of China (10721062, 11072051, 90715037 and 51021140004), the National Key Basic Research Special Foundation of China (2010CB832704), the 111 Project (No. B08014) and the Australian Research Council (ARC LX0989423) are gratefully acknowledged.

References

[1] F.P. Incropera, D.P. DeWitt, T.L. Bergman, A.S. Lavine, Fundamentals of Heat and Mass Transfer, sixth ed, John Wiley & Sons, New York, 1979.
[2] W. Woodside, J.H. Messmer, Thermal conductivity of porous media I unconsolidated sands, J. Appl. Phys. 32 (1961) 1688–1698.
[3] S. Tavman, I.H. Tavman, Measurement of effective thermal conductivity of wheat as a function of moisture contact, Int. Commun J. Heat Mass Transfer 25 (1998) 733–741.
[4] K. Bala, P.R. Pradhan, N.S. Saxena, Effective thermal conductivity of copper powders, J. Phys. D Appl. Phys. 22 (1989) 1068–1072.
[5] G. Weidenfeld, Y. Weiss, H. Kalman, The effect of compression and preconsolidation on the effective thermal conductivity (ETC) of particulate beds, Powder Technol. 133 (2002) 15–22.
[6] M. Bahrami, M.M. Yovanovich, J.R. Culham, Effective thermal conductivity of rough spherical packed beds, Int. J. Heat Mass Transfer 49 (2006) 3691–3701.
[7] W.L. Vargas, J.J. McCarthy, Stress effects on the conductivity of particulate beds, Chem. Eng. Sci. 57 (2002) 3119–3131.
[8] W.L. Vargas, J.J. McCarthy, Thermal expansion effects and heat conduction in granular materials, Phys. Rev. E 76 (2007) 041301.
[9] K. Chen, J. Cole, C. Conger, J. Draskovic, M. Lohr, K. Klein, T. Scheidemantel, P. Schiffer, Packing grains by thermal cycling, Nature 442 (2006) 257.
[10] V.D. Nguyen, C. Cogné, M. Guessasma, E. Bellenger, J. Fortin, Discrete modeling of granular flow with thermal transfer: application to the discharge of silos, Appl. Therm. Eng. 29 (2008) 1846–1853.
[11] M. Bahrami, M.M. Yovanovich, J.R. Culham, Thermal joint resistances of non-conforming rough surfaces with gas-filled gaps, J. Thermophys Heat Transfer 18 (2004) 326–332.
[12] M. Bahrami, J.R. Culham, M.M. Yovanovich, G.E. Schneider, Review of thermal joint resistance models for non-conforming rough surfaces in a vacuum, Appl. Mech. Rev. 59 (2006) 1–12.
[13] P.A. Cundall, O.D.L. Strack, A discrete numerical model for granular assemblies, Geotechnique 29 (1979) 47–65.
[14] K.L. Johnson, Contact Mechanics, Cambridge University Press, Cambridge, UK, 1987.
[15] L.E. Silbert, D. Ertas, G.S. Grest, T.C. Halsey, D. Levine, S.J. Plimpton, Granular flow down an inclined plane: Bagnold scaling and rheology, Phys. Rev. E 64 (2001) 051302.
[16] M.M. Yovanovich, Thermal contact resistance across elastically deformed spheres, J. Spacecr. Rockets 4 (1967) 119–122.
[17] R. Holm, Electrical Contacts: Theory and Application, Springer-Verlag, New York, 1967.
[18] F.G.K. Batchelor, R.W. O'Brien, Thermal or electrical conduction through a granular material, Proc. R. Soc. London A 355 (1977) 313–333.
[19] A. Jagota, C.Y. Hui, The effective thermal conductivity of a packing of spheres, J. Appl. Mech. 57 (1990) 789–791.
[20] M. Bahrami, J.R. Culham, M.M. Yovanovich, Thermal contact resistance: a scale analysis approach, J. Heat Transfer 26 (2004) 896–905.
[21] L.H. Tanner, M. Fahoum, A study of the surface parameters of ground and lapped metal surfaces using specular and diffuse reflection of laser light, Wear 36 (1976) 299–316.
[22] G. Weidenfeld, Y. Weiss, H. Kalman, A theoretical model for effective thermal conductivity (ETC) of particulate beds under compression, Granular Matter 6 (2004) 121–129.
[23] H.L. Xing, A. Makinouchi, Three dimensional finite element modeling of thermomechanical frictional contact between finite deformation bodies using R-minimum strategy, Comput Method Appl M 191 (2002) 4193–4214.
[24] K. Bagi, Stress and strain in granular assemblies, Mech. Mater. 22 (1996) 165–177.
[25] W. Ehlers, E. Ramm, S. Diebels, G.A. D'Addetta, From particle ensembles to Cosserat Continua: homogenization of contact forces towards stresses and couple stresses, Int. J. Solids Struct. 40 (2003) 6681–6702.
[26] C.S. Chang, M.R. Kuhn, On virtual work and stress in granular media, Internal Int J Solids Struct 42 (2005) 3773–3793.
[27] C.L. Liao, T.P. Chang, D.H. Young, C.S. Chang, Stress–strain relationship for granular materials based on the hypothesis of best fit, Int. J. Solids Struct. 34 (1997) 4087–4100.
[28] B. Cambou, M. Chaze, F. Dedecker, Change of scale in granular materials, Eur. J. Mecha. A/Solids 19 (2000) 999–1014.
[29] M. Satake, Tensorial form definitions of discrete mechanical quantities of granular assemblies, Int. J. Solids Struct. 41 (2004) 5775–5791.
[30] X.H. Wen, L.J. Durlofsky, M.G. Edwards, Use of border regions for improved permeability upscaling, Math. Geol. 35 (2003) 521–547.
[31] H.W. Zhang, Z.D. Fu, Coupling upscaling finite element method for consolidation analysis of heterogeneous saturated porous media, Adv. Water Resour. 33 (2010) 34–47.
[32] K. Chen, J. Lan, Micromorphic modeling of granular dynamics, Int. J. Solids Struct. 46 (2009) 1554–1563.
[33] ABAQUS theory manual, version 6.4, Hibbit, Karlsson and Sorensen Inc., 2003.